Silicon (2022) 14:10817–10826
https://doi.org/10.1007/s12633-022-01784-7

ORIGINAL PAPER

Chemical Composition, Mechanical, and Thermal Characteristics of Bioactive Glass for Better Processing Features

Kh. S. Shaaban[1] · B. M. Alotaibi[2] · Saud A. Algarni[3] · Nuha Alharbiy[4] · E. A. Abdel Wahab[5]

Received: 27 December 2021 / Accepted: 17 February 2022 / Published online: 19 March 2022
© The Author(s), under exclusive licence to Springer Nature B.V. 2022

Abstract

Glass system was designed using the formula $34B_2O_3 - 9SiO_2 - 18CaO - 14\ P_2O_5 - (25 - x)\ Na_2O$ - $xTiO_2$, $x = (0 \leq x \leq 5$ mol%) in this article. Glass systems were investigated in terms of physical, structural, thermal, and mechanical characteristics. Furthermore, XRD was used to characterize amorphous nature systematically. The structural networks in the samples were analyzed by FTIR spectra to illustrate structural units like SiO_4, TiO_4, BO_3, and BO_4. Titanium ions act as a trigger to convert BO_3 into BO_4 units, according to preliminary FT-IR results. The glass density and velocities increased after adding TiO_2. The experimental and theoretical elastic moduli increased with increasing glass densities and velocities. The increasing trend of ΔT with increasing TiO_2 concentration suggested that glass stability had enhanced. According to the results of this study, the mechanical and thermal features of the bioactive glass compositions studied are significantly influenced by the addition of TiO_2. This research could be used in the future to improve the mechanical and thermal efficiency of bioactive glass systems. G 5 is the best one in terms of mechanical and thermal properties according to these findings.

Keywords Bioactive glass · Mechanical · DTA · FT-IR

1 Introduction

Biocompatible materials for implant applications have gotten a lot of attention in recent years [1–7]. In dental prosthetics and orthopedic implants, as a filler material, bioactive glasses are used. The existence of bioactive glasses with a variety of physicochemical and mechanical characteristics expands the variety of potential therapeutic options. It has been attempted to describe the impacts of thermal treatment conditions and bioactivity [8–12].

45S5 is the most commonly used bioactive glass for many applications [13, 14]. When B_2O_3 is added to 45S5 bioglass, the glass's acellular bioactive behavior improves as a result. Sitarz et al. [15] and his associates used SEM, EDAX, MIR, and NMR procedures to investigate the bioactivity of B_2O_2 mixed $NaCaPO_4$–SiO_2–PO_4 glasses. Several efforts have been made in recent years to modify the chemical composition of bioactive glasses to control the rate of degradation and mechanical strength and incorporate other oxides like Na_2O, CaO, Al_2O_3, and TiO_2 into the bioactive glass [16–18]. The elastic properties of biomaterials have been measured using various techniques, for instance, ultrasonic procedures. The ultrasonic non-destructive method procedure has long been regarded as a one-of-a-kind tool for determining the properties of materials.

The presence of TiO_2 in glasses has a significant impact on structural, physical, and thermodynamic properties, including polymerization degree [5, 10, 19–30]. Duan et al. [31] & Moghanian et al. [32–41] examined the mechanism

✉ Kh. S. Shaaban
khamies1078@yahoo.com

✉ Nuha Alharbiy
nfharbiy@uqu.edu.sa

[1] Department of Chemistry, Faculty of Science, Al - Azhar University, P.O. 71452, Assiut, Egypt

[2] Physics Department, College of Science, Princess Nourah bint Abdulrahman University, P.O. Box 84428, Riyadh 11681, Saudi Arabia

[3] Department of Physics, College of Science, Taif University, P.O. Box 11099, Taif 21944, Saudi Arabia

[4] Physics Department, Faculty of Science, Umm Al-Qura University, Makkah, Saudi Arabia

[5] Physics Department, Faculty of Science, Al-Azhar University, P.O. 71524, Assiut, Egypt

of TiO_2's role in the $CaO–Al_2O_3–SiO_2–TiO_2$ glass structure. Bioglass-based medical products in orthopedics and dentistry are the most common. These glasses have been studied in terms of a variety of factors, including modifying a chemical formulation. Thermal stability and mechanical characteristics were found to increase as the concentration of TiO_2 increased, indicating the formation of oxygen bridges (BO). Herein, we are focusing on the XRD, FT-IR, DTA, and ultrasonic velocities of the glass samples which are not yet widely studied. The relevant information here is used to determine the optimal glass composition for biomedical applications. The high reactivity of these materials is their primary benefit for periodontal repair and bone augmentation.

2 Methods and Materials

Preparation: $34B_2O_3 – 9SiO_2 – 18CaO – 14\ P_2O_5 – (25 – x)\ Na_2O$ - $xTiO_2$, $x = (0 \le x \le 5$ mol%) glass in Table 1 and ref. [42] was prepared.

XRD& Density measurements: As ref. [42].

FT-IR: A JASCO 430 spectrometer was used to detect FT-IR absorption.

DTA: A Thermal Analyzer (TA-50 Shimadzu, Japan) was utilized to perform differential thermal analysis (DTA). The glass transition, onset crystallization, and fully crystallization temperatures T_g, T_c, & T_p for each glass were determined using the general procedure for determining T_g, T_c, and $T_p$for each glass.

Mechanical: The Echo - graph (Krautkramer model USM3) was used to make the ultrasonic measurements.

The longitudinal and shear V_L&V_T velocities were calculated using this method. In addition to the density, the V_L&V_T were accustomed to calculating elastic moduli.

Longitudinal : $L = \rho v_l^2$,

Transverse, $G = \rho v_t^2$,

Young's : $Y = (1 + \sigma)2G$.

Table 1 Chemical formulation (mol, %)

code	B_2O_3	SiO_2	CaO	P_2O_5	Na_2O	TiO_2
G 1	34	9	18	14	25	0
G 2	34	9	18	14	24	1
G 3	34	9	18	14	23	2
G 4	34	9	18	14	22	3
G 5	34	9	18	14	20	5

Bulk : $K = L - \left(\frac{4}{3}\right)G$.

Dimensionality $d = \left({}^{G}/_{K}\right)$*4.

Hardness; $H = \frac{(1-2\sigma)Y}{6(1+\sigma)}$.

Debye, $\theta_D = \frac{h}{k}\left(\frac{9N}{4\pi V_m}\right)^{\frac{1}{3}} M_s$.

Velocity averages $M_s = \frac{1}{3}\left(\frac{\frac{2}{v_T^3}}{\frac{1}{v_l^3}}\right)^{\frac{1}{3}}$,

Expansion of the thermal $\alpha_{P=23.2\ (v_L-0.57457)}$,

oxygen's molar volume $V_o = \left(\frac{M}{\rho}\right)\left(\frac{1}{\sum xini}\right)$,

Oxygen packing density $OPD = \left(\frac{1000\ C}{Vm}\right)\left(\frac{Mol}{L}\right)$.

The acoustic impedance; $Z = v_L\rho$.

Softening temperature : $T_s = \frac{M*(V_l*100)^2}{\sum_i x_i X_i*(50740)^2}$

The dissociation energy (Gi) and packing density(V_i) are used in the elastic module's theoretical calculations.

(V_i) are used. $V_i = \left(\frac{3\pi}{4}\right)NA\left\{mR^3 + n\ R_i^3\right\}\left(\frac{m^3}{mol}\right)$,

$Gi = \left(\frac{1}{V_m}\right)\sum_i GiXi$.

The ratio of Poisson's, $\sigma = \frac{1}{2} - \left(\frac{1}{7.2*Vi}\right)$.

3 Results and Discussion

3.1 Physical Characteristics

XRD pattern proves that the glasses have an amorphous state [22, 42–48] (Fig. 1). Density (ρ) and molar volume (V_m) are used to examine the physical characteristics of glasses. All of the prepared samples' (ρ) and (V_m) values are shown in Fig. 2. G 5 has a significantly higher density than the others. The difference in molecular masses and densities between TiO_2 (79.89 g/mol),(4.23 g. cm^{-3}) and Na_2O (61.69 g/mol), (2.27 g. cm^{-3}) explains the increase in (ρ) with increasing TiO_2 content. Furthermore, the increase in (ρ) denotes that TiO_2 causes the glass structure to become more compact. It has been discovered that the values of (V_m) are lower. This may be due to a decrease in interatomic spacing between the glass networks, which causes a decrease in V_m. G 5 has a

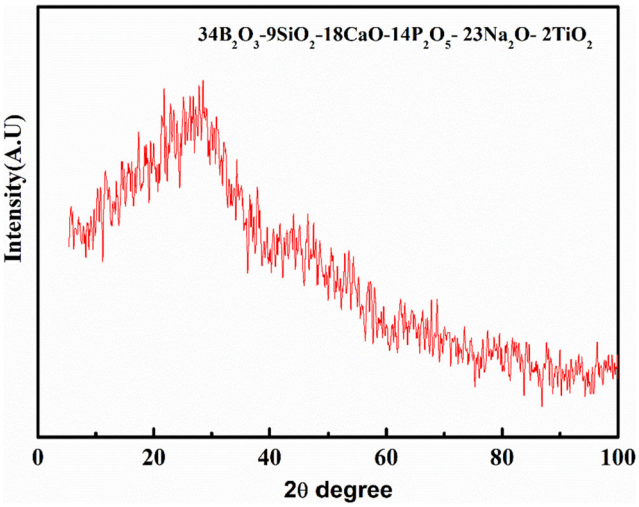

Fig. 1 XRD of $34B_2O_3$-$9SiO_2$- 18CaO – $14P_2O_5$ – $23Na_2O$- $2TiO_2$ glass sample

significantly lower V_m than the others. The variation in bond length between Ti- Ti (0.2896 nm) and Na_2O (0.3716 nm) explains the decrease in V_m with increasing TiO_2 content [49–56]. As a result, such behavior denotes the presence of BO as a result of TiO_2 substitution. As a result, the values (ρ) and (V_m) of this study agree with the values (ρ) and (V_m) of the calculated El-Maaref et al. [49, 52].

3.2 DTA

The T_g, T_c, & T_p temperatures are parameters that depend on bond strength, cross-link density, and packing density. The relationship between the glass structure and the glass characteristics is reflected in these temperatures [11, 57, 58]. The constructional dependence on TiO_2 amount in the $34B_2O_3$ – $9SiO_2$ – 18CaO – 14 P_2O_5 – $(25 - x)$ Na_2O - $xTiO_2$, $x = (0 \leq x \leq 5$ mol%) glasses is the most noticeable feature. The DTA profile for all of the samples is shown in Fig. 3 & Table 2. It can be seen in Table 2 that the T_g, T_c, & T_p increases as the

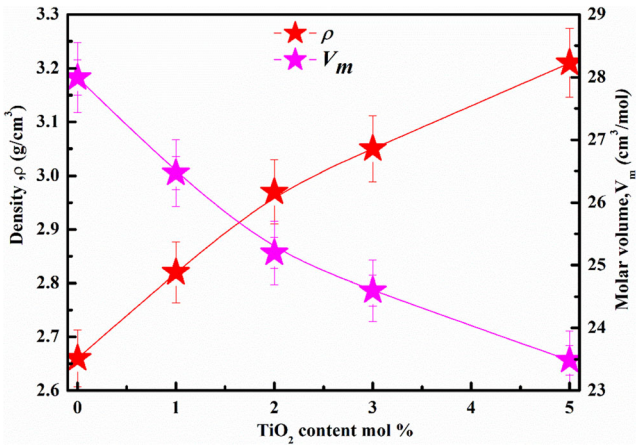

Fig. 2 ρ & $V_m$of synthetic samples

Table 2 DTA data of investigated glasses

code	T_p (K)	T_g (K)	ΔT	T_c (K)	S	Hg
G 1	951.15	727.15	224	860.15	28.03	0.308
G 2	983.15	748.15	235	889.15	29.53	0.314
G 3	1008.15	754.15	254	909.15	33.34	0.337
G 4	1018.15	771.15	247	924.15	30.11	0.32
G 5	1052.15	788.15	264	950.15	34.17	0.335

TiO_2 content rises. We expose all evidence that validates our description in this work to test the dependence T_g, T_c, & T_p has on other parameters. Because the bond strength of Ti-O (73kcals) is higher than that of Na-O (20 kcals), the T_g, T_c, & T_p *values* increases with TiO_2.

The thermal stability of the glasses ($\Delta T = T_c - T_g$), weighted thermal stability $H_g = \frac{\Delta T}{T_g}$, S criterion $S = (T_p - T_c)\frac{\Delta T}{T_g}$. ΔT, H_g, and S values increases as the TiO_2 content increases. The most thermally stable glass is the one with the highest TiO_2 content. The term ΔT specifies the glasses' thermal stability, and we reported that ΔT values rise as TiO_2 content rises. The increasing trend of ΔT with increasing TiO_2 concentration, on the other hand, suggested that glass stability had enhanced. As the replacement of weaker Na-O bonds by stronger Ti-O bonds can be attributed to the increasing glass stability as TiO_2 increases. These results are identical to those obtained from the data in [59–61]. As a result, such behavior denotes the presence of BO as a result of TiO_2 substitution. As a result, the values T_g, T_c, & T_p, ΔT, H_g & S of this study agree with the values calculated by Alrowaili et al. & Wahab et al. [52, 59].

We calculated the (*OPD*) to study the effect of TiO_2 content on T_g, as shown in Table 2, and Fig. 4. The increase in T_g could be explained by the (OPD) parameter, as shown in

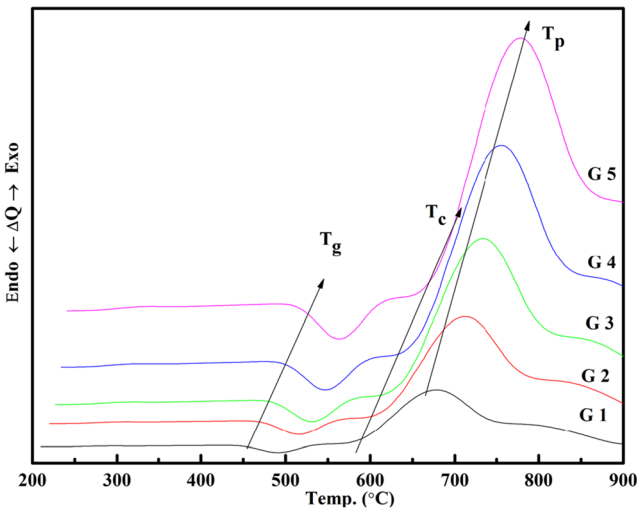

Fig. 3 DTA of investigated glasses

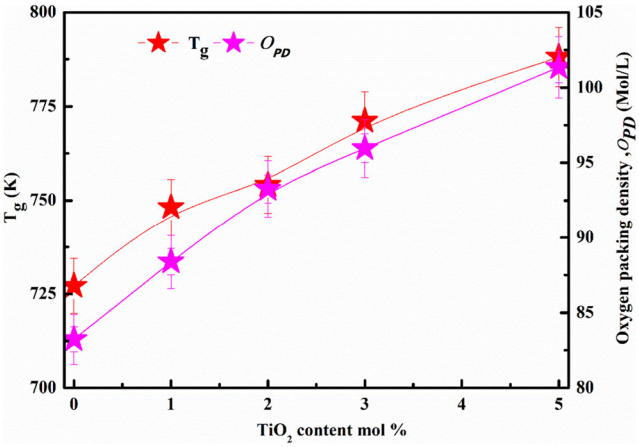

Fig. 4 (O_{BD}) & (T_g) of synthetic samples

Fig. 4. It exhibited a similar trend to that of T_g as TiO_2 content increased. We can deduce that the bond strength and *OPD* parameters control the variation of T_g based on these two parameters. By forming TiO_x (x = 4 or 6), we can link an increase in T_g to an increment in network connectivity. We propose that the titanium structural units in the glass network result in higher connectivity based on the chemical formula $34B_2O_3 - 9SiO_2 - 18CaO - 14\ P_2O_5 - (25 - x)\ Na_2O$ - $xTiO_2$, $x = (0 \le x \le 5$ mol%). As a result, when TiO_2 increases, the T_g value of the glasses increment. The rigidity of the glass network increased as a result of the cross-linking, resulting in an increment in T_g [59–61].

3.3 Mechanical Investigations

Figure 5 and Table 3 present the experimental values of ultrasonic velocities (V_L & V_T) as well as various glass compositions. Table 3& Fig. 5 show that adding more TiO_2 content increases velocities. V_L values range from 4590 to 5040 m/s, while V_T values range from 2435 to 2610 m/s. With more TiO_2 added, the composition-dependent density increases (V_L & V_T), as shown in Fig. 5. The increase in (V_L & V_T), as TiO_2 content increases, may be due to an increase in bonding oxygen (BO) and, as a result, the glass network's connectivity. Furthermore, the increase in (V_L & V_T), confirm that TiO_2 causes the glass structure to become more compact [51, 62–67]. These results are identical to those obtained from the data in [51, 62–67]. As a result, such behavior denotes the generation of BO with TiO_2 substitution. The values of this study agree with the values calculated by El-Rehim et al., Koubisy et al. & Alothman et al. [62, 63, 65].

With the addition of TiO_2, all elastic moduli (both experimentally and theoretically) show the same trend of variations across the entire composition range, as shown in Figs. 6, 7 & Table 3. All elastic moduli were an effect by ρ, V_L & V_T. When the Na_2O glass is modified with TiO_2, the increment

Table 3 Mechanical parameters values

Samples	G 1	G 2	G 3	G 4	G 5
V_L	4590	4705	4820	4895	5040
V_T	2435	2460	2545	2565	2610
L	56.04	62.43	69.00	73.08	81.54
G	15.77	17.07	19.24	20.07	21.87
K	35.01	39.67	43.35	46.33	52.38
Y	41.14	44.77	50.27	52.6	57.59
L_{th}	155.65	173.67	191.76	202.93	226.44
G_{th}	35.58	37.99	40.33	41.85	44.96
K_{th}	108.21	123.02	137.99	147.13	166.49
Y_{th}	91.14	97.90	104.46	108.65	117.23
V_i	0.99	1.05	1.10	1.13	1.19
G_i	10.98	11.15	11.31	11.48	11.81
V_o	12.02	11.31	10.72	10.42	9.87
O_{PD}	83.23	88.40	93.27	95.96	101.36
d	1.80	1.72	1.77	1.73	1.67
T_s	422	432	464	472	491
α_p	106,475	109,143	111,811	113,551	116,915
H	2.06	2.14	2.48	2.53	2.67
M_s	1886.8	1908.1	1972.7	1989.2	2025.7
θ_D	359.4	370.3	389.2	395.6	409.2
Z	1.2	1.3	1.4	1.5	1.6

in elastic moduli is proportional to the increase in sample densities, indicating that Ti ions fill the interstitial positions of the Na glass network [51, 62–67].

As the TiO_2 content increases, the (d), (H), (σ), and (Z) increase as well, reaching a maximum of 5 mol% TiO_2, as shown in Fig. 8. The glasses under investigation have a (d) parameter of around 2, indicating a two-dimensional structure with growing cross-links. The Poisson's ratio (σ), increases as TiO_2 increases (σ), is the ratio of horizontal to longitudinal strain in a glass system, and it is usually proportional to the

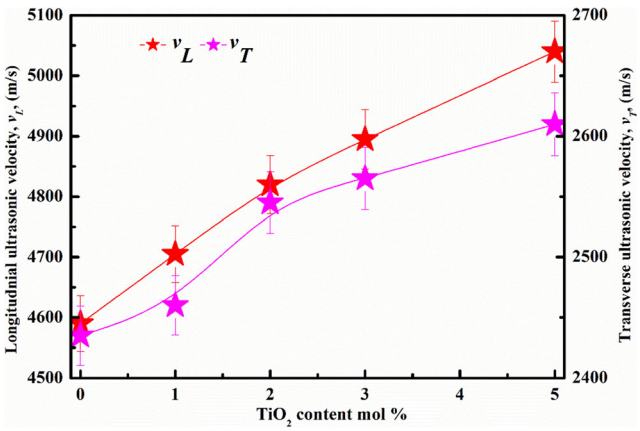

Fig. 5 V_L & V_T of manufactured samples

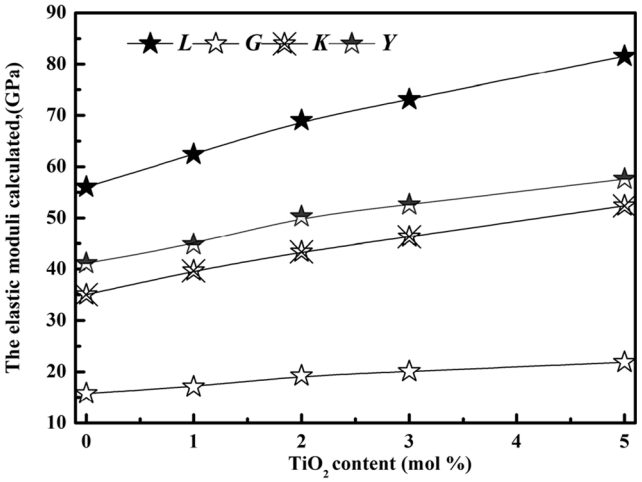

Fig. 6 *L. G. K & Y* experimentally for glasses

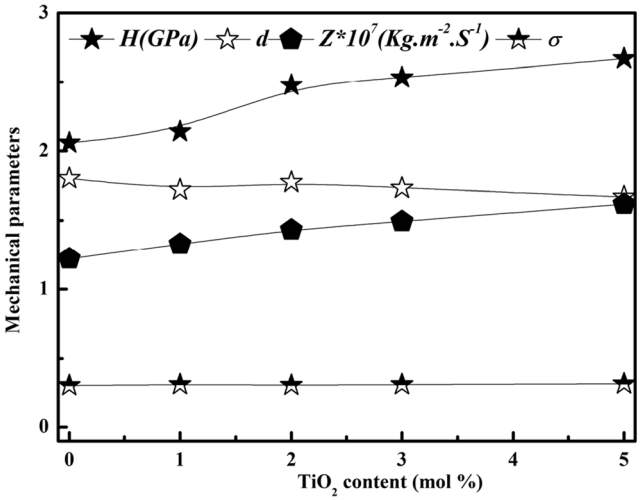

Fig. 8 (*d*), (*H*), (σ)& (*Z*) for glasses

true crosslink density. (σ), increases as the average crosslink density rise. The Debye temperatures (θ_D) and average velocities M_s s of TiO_2 -containing glass samples are shown in Fig. 9. (θ_D) is dependent on (M_s). As a direct consequence, θ_D increased as TiO_2 content increased. Fig. 10 shows the *Ts* &αp for each sample. The addition of TiO_2 enhances *Ts* &αp, as previously stated. (V_i) and (G_i) refer to the investigated TiO_2-containing glasses, as shown in Fig. 11. (V_i) and (G_i) values increment as TiO_2 increment [51, 62–67]. These values are illustrated in Table 3. These results are identical to those obtained from the data in [51, 62–67].

3.4 FT-IR Characteristics

The boron in the glasses originated in various vibrational states, as shown in the FT-IR spectra Fig. 12. Furthermore, in many areas of the spectrum, SiO_4 and BO_4 units overlap significantly [3, 4, 21, 45, 68–72]. The bands between 1200 and 1400 cm^{-1} are related to various (B-O stretching) vibrations, and the absorption at 745 cm^{-1} belongs to (B-O bending). The presence of BO_4 and BO_3 of boron is represented by these bands. Shoulders amongst 865 cm^{-1} and 1200 cm^{-1} on

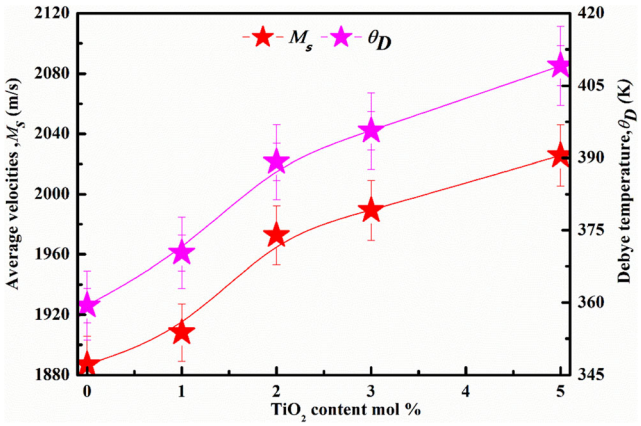

Fig. 9 (θ_D) & (M_s),for glasses

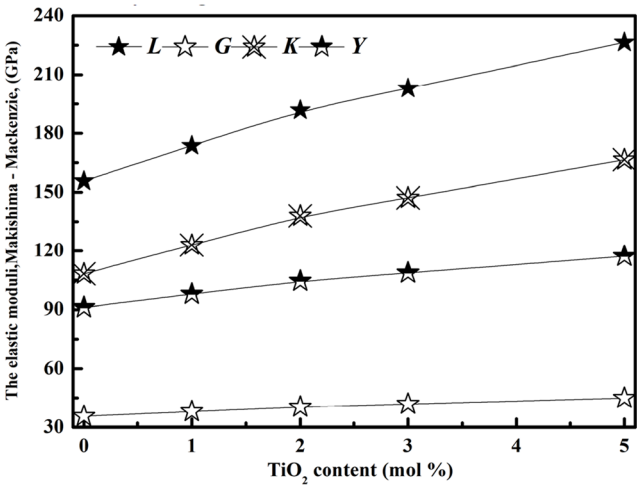

Fig. 7 *L. G. K & Y* theoretically for glasses

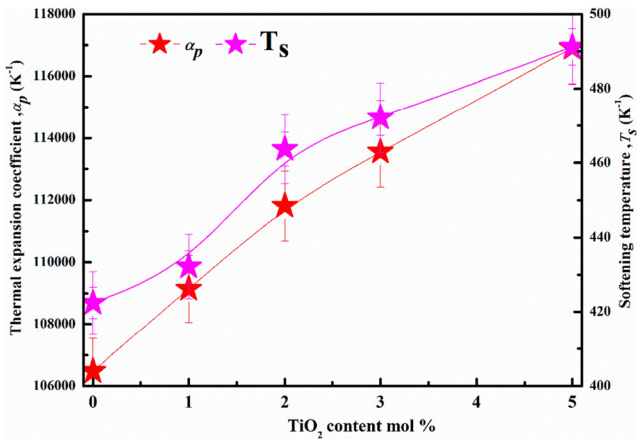

Fig. 10 *Ts* &αp for glasses

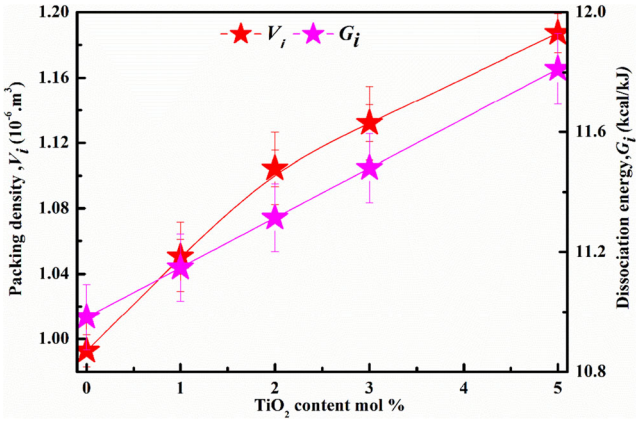

Fig. 11 (V_i) and (G_i) for glasses

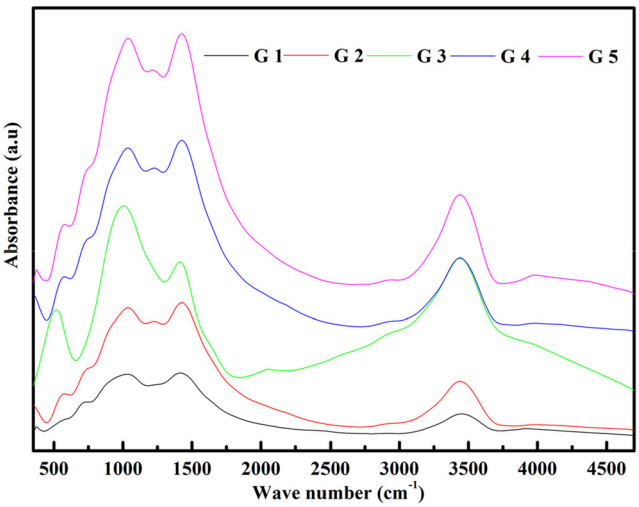

Fig. 12 FT-IR of manufactured samples

the other hand, specify the establishment of BO_4. However, because of Si-O and P-O bonds. Bands at 374–392^{-1} due to the vibration of metal cation as Ti^{+2}, Ca^{+2},& Na^{+}. The Si-O-Si bond vibration, which belongs to the (SiO_4) units, is responsible for the band at 442 - 405 cm^{-1}. The TiO_4 bond vibrations are responsible for the band at ~532 cm^{-1}. The (P-O) bond is responsible for the absorption between 570 cm^{-1}. Furthermore, (Si-O-NBO) bonds can be attributed to the bands in the 1174–952 cm^{-1} region. Band of 952 cm^{-1} is correlated to O –Ti– O in [Si(Ti)O_4] tetrahedral. Hydrogen bonding is caused by vibrations between ~2887 cm^{-1}. H_2O is responsible for the vibrations seen at ~3435 cm^{-1}. B can change its coordination number with oxygen from BO_3 to BO_4, resulting in a variety of anionic environments in which the modifying metal ions can coordinate. The addition of dopants to boroxide glass makes the structure more stable, which can be deduced.

The effect of titanium ions on the relative of BO_4 and BO_3 was calculated using the deconvolution parameters, such as relative area (A) of FT-IR peaks. The de-convoluted FT-IR spectrum is shown in Fig. 13. For each glass sample, Table 4 lists de-convolution parameters. To calculate the fraction of N_4 & N_3 values, use the following formulas:

$$N_4 = \frac{A1}{A1 + A2},$$

$$N_3 = 1 - N_4$$

The increase in N_4values correspond to a rise in BO_4 units and the decrease in N_3 values correspond to a reduction in BO_3 units. BO_3 and BO_4 units coexist in the glass composition, according to FT-IR spectra. Titanium ions appear to convert trigonal BO_3 units into tetrahedral BO_4 units, according to preliminary FT-IR results [3, 4, 21, 45, 68–72].

4 Conclusions

The physical, thermal, and mechanical characteristics of glass systems $34B_2O_3 - 9SiO_2 - 18CaO - 14\ P_2O_5 - (25 - x)$ Na_2O - $xTiO_2$, $x = (0 \le x \le 5$ mol%) were investigated. The absence of peaks in the XRD spectra signifies the amorphous phase of the fabricated samples. The structural network in the samples was confirmed by FTIR spectra to contain structural units like SiO_4, TiO_4, BO_3, and BO_4. Titanium ions appear to

Table 4 De-convolution parameters of the glasses under investigation

G 1	C	374	–	570	713	869	986	1072	–	1210	1410	(A1)	(A2)	N_4	N_3
	A	2.79	–	13.35	7.03	23.36	16.57	10.57	–	15.57	10.75	50.504	26.323	0.657	0.343
G 2	C	–	405	559	721	868	966	1055	–	1206	1413				
	A	–	3.01	10.49	13.98	17.35	17.32	14.84	–	14.69	8.31	49.507	23.009	0.683	0.317
G 3	C	–	442	532	745	883	992	1081	–	1235	1418				
	A	–	9.37	10.46	8.31	13.78	20.81	15.38	–	13.50	8.39	49.973	21.891	0.695	0.305
G 4	C	392	–	558	720	885	–	1035	1132	1235	1410				
	A	4.50	–	8.58	14.10	17.71	–	23.79	12.64	9.21	9.48	54.132	18.687	0.743	0.257
G 5	C	378	–	567	729	864	952	1045	1174	–	1419	63.257	7.394	0.895	0.105
	A	2.90	–	12.29	14.17	11.97	12.88	10.42	27.98	–	7.39				

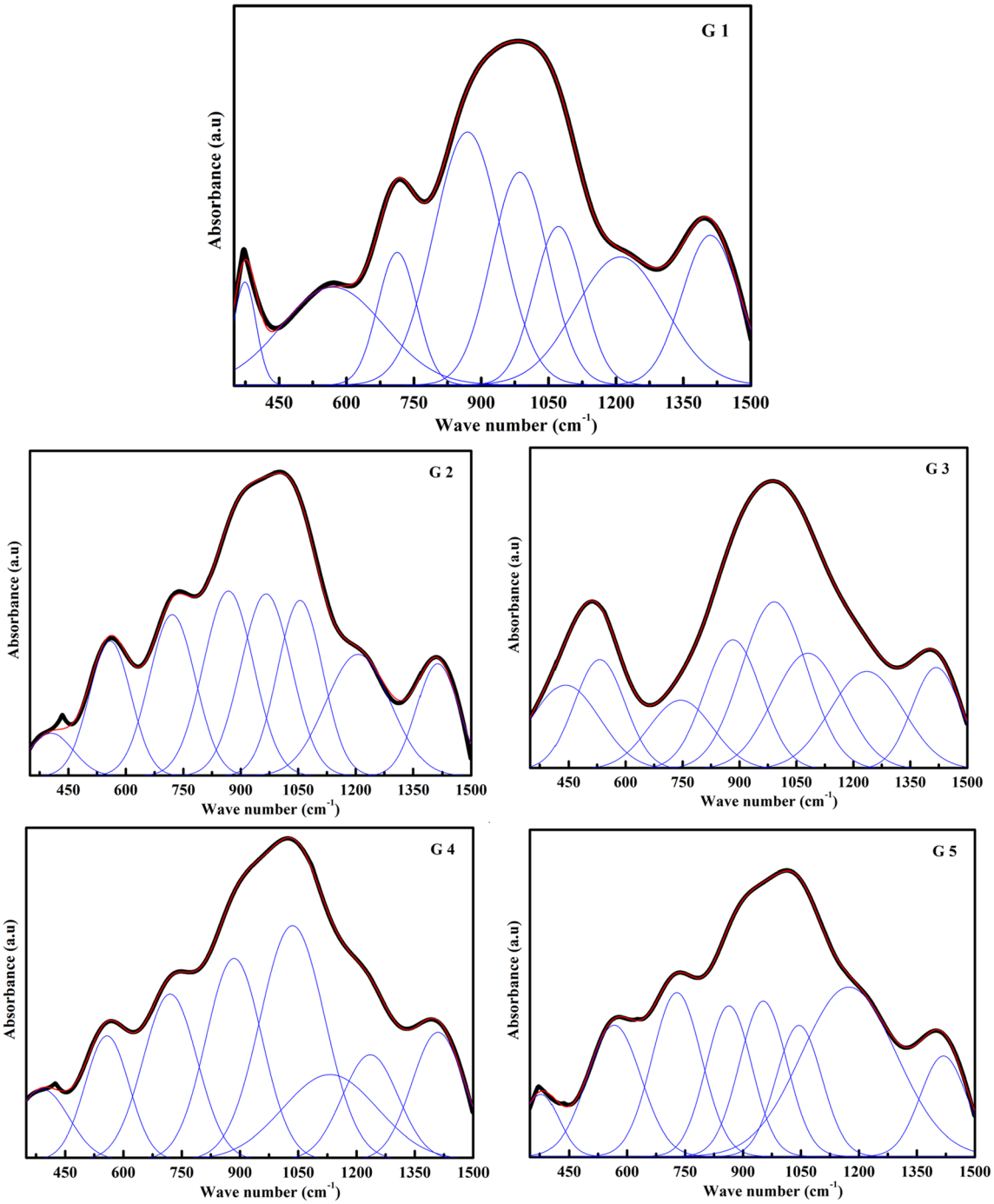

Fig. 13 De-convoluted FT-IR spectrum

convert BO_3 into BO_4 units, according to preliminary FT-IR results. The glass density and velocities increased after TiO_2 was added. The experimental and theoretical elastic moduli increase with increasing glass densities and velocities. The increasing trend of ΔT with increasing TiO_2 concentration suggested that glass stability had enhanced. According to the results of this study, the mechanical and thermal properties of the bioactive glass compositions studied are significantly influenced by the addition of TiO_2. This research could be used in the future to enhance the mechanical and thermal efficiency of bioactive glass systems.

Acknowledgments The authors express their gratitude to princess Nourah bint Abdulrahman University, Researchers Supporting Project (Grant No. PNURSP2022R32) Princess Nourah bint Abdulrahman University, Riyadh, Saudi Arabia. Moreover, we would like to thank Taif University Researchers Supporting Project number (TURSP-2020/250), Taif University, Taif, Saudi Arabia.

Author Contributions All of the authors have taken full responsibility for the content of this manuscript.

Data Availability My manuscript and associated personal data.

Compliance with Ethical Standards The manuscript has not been published elsewhere.

Conflict of Interest The authors declare that they have no conflict of interest.

Declaration of Competing Interest There are no known competing financial interests among the authors.

Consent to Participate & Publication The author's consent to participate & publication.

References

1. Rajkumar G, Aravindan S, Rajendran V (2010) Structural analysis of zirconia-doped calcium phosphate glasses. J Non-Cryst Solids 356:1432–1438. https://doi.org/10.1016/j.jnoncrysol.2010.05.003
2. Shaaban KS, Yousef ES (2020) Optical properties of Bi_2O_3 doped boro tellurite glasses and glass ceramics. Optik 203:163976. https://doi.org/10.1016/j.ijleo.2019.163976
3. El-Rehim AFA, Zahran HY, Yahia IS, Makhlouf SA, Shaaban KS (2021) Radiation, crystallization, and physical properties of cadmium borate glasses. Silicon 13:2289–2307. https://doi.org/10.1007/s12633-020-00798-3
4. El-Rehim AFA, Zahran HY, Yahia IS, Ali AM, Shaaban KS (2020) Physical, radiation shielding and crystallization properties of Na_2O-Bi_2O_3- MoO_3-B_2O_3- SiO_2-Fe_2O_3 glasses. Silicon. 14:405–418. https://doi.org/10.1007/s12633-020-00827-1
5. Shaaban KS, Yousef ES, Mahmoud SA, Wahab EAA, Shaaban ER (2020) Mechanical, structural and crystallization properties in Titanate doped phosphate glasses. J Inorg Organomet Polym Mater 30:4655–4663. https://doi.org/10.1007/s10904-020-01574-x
6. Shaaban KS, Al-Baradi AM, Alrowaili ZA, Ali AM, Al-Buriahi MS, Wahab EAA (2021) Structural, thermal, and mechanical characteristics of yttrium lithium borate glasses and glass–ceramics. J Mater Sci Mater Electron 32:28065–28075. https://doi.org/10.1007/s10854-021-07158-w
7. El-Rehim AFA, Wahab EAA, Halaka MMA, Shaaban KS (2021) Optical properties of SiO_2 – TiO_2 – La_2O_3 – Na_2O – Y_2O_3 glasses and a novel process of preparing the parent glass-ceramics. Silicon. 14:373–384. https://doi.org/10.1007/s12633-021-01002-w
8. Fujibayashi S (2003) A comparative study between in vivo bone ingrowth and in vitro apatite formation on Na_2O–CaO–SiO_2 glasses. Biomaterials 24:1349–1356. https://doi.org/10.1016/s0142-9612(02)00511-2
9. Begum AN, Rajendran V, Ylänen H (2006) Effect of thermal treatment on physical properties of bioactive glass. Mater Chem Phys 96:409–417. https://doi.org/10.1016/j.matchemphys.2005.07.031
10. Shaaban KS, Alrowaili ZA, Al-Baradi AM, Ali AM, Wahab EAA, Al-Buriahi MS (2021) Mechanical and thermodynamic characteristics of 22SiO_2- 23Bi_2O_3-37B_2O_3-13TiO_2-(5-x) LiF- x BaO glasses. Silicon. https://doi.org/10.1007/s12633-021-01441-5
11. Shaaban KS, Alomairy S, Al-Buriahi MS (2021) Optical, thermal and radiation shielding properties of B_2O_3–NaF–PbO–BaO–La_2O_3 glasses. J Mater Sci Mater Electron 32:26034–26048. https://doi.org/10.1007/s10854-021-05885-8
12. Nabian N, Delavar M, Rabiee MS, Jahanshahi M (2013) Quenched/unquenched nanobioactive glass-ceramics: synthesis and in vitro bioactivity evaluation in Ringer's solution with BSA. Chemical Industry and Chemical Engineering Quarterly/CICEQ 19(2):231–239. https://doi.org/10.2298/CICEQ120323057
13. Hench LL (1991) Bioceramics: from concept to clinic. J Am Ceram Soc 74:1487–1510. https://doi.org/10.1111/j.1151-2916.1991.tb07132.x
14. Fiume E, Barberi J, Verné E, Baino F (2018) Bioactive glasses: from parent 45S5 composition to scaffold-assisted tissue-healing therapies. J Functional Biomaterials 9:24. https://doi.org/10.3390/jfb9010024
15. Sitarz M, Bulat K, Olejniczak Z (2012) Structure and microstructure of glasses from a $NaCaPO_4$–SiO_2–BPO_4 system. Vib Spectrosc 61:72–77. https://doi.org/10.1016/j.vibspec.2012.01.016
16. Mohini GJ, Krishnamacharyulu N, Sahaya Baskaran G, Rao PV, Veeraiah N (2013) Studies on influence of aluminium ions on the bioactivity of B_2O_3–SiO_2–P_2O_5–Na_2O–CaO glass system by means of spectroscopic studies. Appl Surf Sci 287:46–53. https://doi.org/10.1016/j.apsusc.2013.09.055
17. Ghorbanzade Zaferani SP, Nabian N, Delavar M, Rabiee SM (2021) Novel methods for adding metal oxides nanoparticles to bioactive glass 58S matrix: a characterization and bioactivity evaluation study. Silicon. https://doi.org/10.1007/s12633-021-01487-5
18. Ghorbanzade Zaferani SP, Nabian N, Delavar M, Rabiee SM (2021) Direct impregnation of MgO nanoparticles in 58S bioactive glass: bioactivity evaluation and antibacterial activity, Iranian journal of science and technology. Transactions A: Science 45(3):885–898. https://doi.org/10.1007/s40995-021-01103-6
19. Saneei Siavashy O, Nabian N, Rabiee SM (2021) Titanium dioxide nanotubes incorporated bioactive glass nanocomposites: synthesis, characterization, bioactivity evaluation and drug loading. Int J Eng 34(1). https://doi.org/10.5829/ije.2021.34.01a.01
20. Dahshan A, Saddeek YB, Aly KA, Shaaban KHS, Hussein MF, Abo El Naga AO, Shaban SA, Mahmoud SO (2019) Preparation and characterization of $Li_2B_4O_7$ – TiO_2 – SiO_2 glasses doped with metal-organic framework derived nano-porous Cr_2O_3. J Non-Cryst Solids 508:51–61. https://doi.org/10.1016/j.jnoncrysol.2019.01.002
21. Alomairy S, Aboraia AM, Shaaban ER, Shaaban KS (2021) Comparative studies on spectroscopic and crystallization properties of Al_2O_3 -Li_2O- B_2O_3-TiO_2 glasses. Braz J Phys 51:1237–1248. https://doi.org/10.1007/s13538-021-00928-1
22. Alharbi T, Mohamed HFM, Saddeek YB, El-Haseib AY, Shaaban KS (2019) Study of the TiO_2 effect on the heavy metals oxides borosilicate glasses structure using gamma-ray spectroscopy and positron annihilation technique. Radiat Phys Chem 164:108345. https://doi.org/10.1016/j.radphyschem.2019.108345
23. Mahmoud KH, Alsubaie AS, Wahab EAA, Abdel-Rahim FM, Shaaban KS (2021) Research on the effects of yttrium on bismuth Titanate borosilicate glass system. Silicon. https://doi.org/10.1007/s12633-021-01125-0
24. Shaaban KS, Boukhris I, Kebaili I, Al-Buriahi MS (2021) Spectroscopic and attenuation shielding studies on B_2O_3-SiO_2-LiF-ZnO-TiO_2 glasses. Silicon. https://doi.org/10.1007/s12633-021-01080-w
25. Shaaban KS, Al-Baradi AM, Wahab EAA (2021) The impact of Y_2O_3 on physical and optical characteristics, polarizability, optical basicity, and dispersion parameters of B_2O_3 – SiO_2 – Bi_2O_3 – TiO_2 glasses. Silicon. https://doi.org/10.1007/s12633-021-01309-8
26. Al-Baradi AM, El-Rehim AFA, Alrowaili ZA, Al-Buriahi MS, Shaaban KS (2021) FT-IR and gamma shielding characteristics of 22SiO_2- 23Bi_2O_3-37B_2O_3-13TiO_2-(5-x) LiF- x BaO glasses. Silicon. https://doi.org/10.1007/s12633-021-01481-x
27. Ali AM, Alrowaili ZA, Al-Baradi AM, Al-Buriahi MS, Wahab EAA, Shaaban KS (2021) A study of thermal, and optical

properties of $22SiO_2$- $23Bi_2O_3$-$37B_2O_3$-$13TiO_2$-(5-x) LiF- x BaO glasses. Silicon. https://doi.org/10.1007/s12633-021-01440-6
28. Shaaban KS, Koubisy MSI, Zahran HY, Yahia IS (2020) Spectroscopic properties, electronic polarizability, and optical basicity of titanium–cadmium tellurite glasses doped with different amounts of lanthanum. J Inorg Organomet Polym Mater 30:4999–5008. https://doi.org/10.1007/s10904-020-01640-4
29. Saddeek YB, Aly KA, Shaaban KS, Ali AM, Sayed MA (2019) The effect of TiO_2 on the optical and mechanical properties of heavy metal oxide borosilicate glasses. Silicon 11:1253–1260. https://doi.org/10.1007/s12633-018-9912-2
30. El-Rehim AFA, Zahran HY, Yahia IS, Wahab EAA, Shaaban KS (2021) Structural, elastic moduli, and radiation shielding of SiO_2-TiO_2-La_2O_3-Na_2O glasses containing Y_2O_3. J Mater Eng Perform 30:1872–1884. https://doi.org/10.1007/s11665-021-05513-w
31. Duan R-G, Liang K-M, Gu S-R (1998) Effect of changing TiO_2 content on structure and crystallization of CaO-Al_2O_3-SiO_2 system glasses. J Eur Ceram Soc 18:1729–1735. https://doi.org/10.1016/s0955-2219(98)00105-8
32. Moghanian A, Nasiripour S, Miri Z, Hajifathali Z, Hosseini SH, Sajjadnejad M, Aghabarari R, Nankali N, Miri AK, Tahriri M (2021) Structural and in vitro biological evaluation of sol-gel derived multifunctional Ti+4/Sr+2 co-doped bioactive glass with enhanced properties for bone healing. Ceram Int 47:29451–29462. https://doi.org/10.1016/j.ceramint.2021.07.113
33. Moghanian A, Koohfar A, Hosseini S, Hosseini SH, Ghorbanoghli A, Sajjadnejad M, Raz M, Elsa M, Sharifianjazi F (2021) Synthesis, characterization and in vitro biological properties of simultaneous co-substituted Ti+4/li+1 58s bioactive glass. J Non-Cryst Solids 561:120740. https://doi.org/10.1016/j.jnoncrysol.2021.120740
34. Amirhossein Moghanian, Mohammadamin Zohourfazeli, Mahzad Haji Mahdi Tajer, Amir K. Miri,(2021) Comprehensive in vitro studies of novel sol gel-derived Zr^{4+}/Zn^{2+} co-substituted bioactive glass with enhanced biological properties for bone healing, journal of non-crystalline Solids,566,120887, https://doi.org/10.1016/j.jnoncrysol.2021.12088
35. Moghanian A, Pazhouheshgar A, Ghorbanoghli A (2021) Nonlinear viscoelastic modeling of synthesized silicate-based bioactive glass/Polysulfone composite: theory and medical applications. Silicon. https://doi.org/10.1007/s12633-020-00900-9
36. Rahmani M, Moghanian A, Saghafi Yazdi M (2021) Synthesis and characterization of in vitro properties and biological behavior of ag/li co-doped 68S bioactive glass with and without phosphate. J Non-Cryst Solids 570:121015. https://doi.org/10.1016/j.jnoncrysol.2021.121015
37. Moghanian A, Tajer MHM, Zohourfazeli M, Miri Z, Yazdi M (2021) Sol-gel derived silicate-based bioactive glass: studies of synergetic effect of zirconium and magnesium on structural and biological characteristics. J Non-Cryst Solids 554:120613. https://doi.org/10.1016/j.jnoncrysol.2020.120613
38. Moghanian A, Nasiripour S, Koohfar A, Sajjadnejad M, Hosseini S, Taherkhani M, Miri Z, Hosseini SH, Aminitabar M, Rashvand A (2021) Characterization, in vitro bioactivity and biological studies of sol-gel-derived TiO_2 substituted 58S bioactive glass. Int J Appl Ceram Technol 18:1430–1441. https://doi.org/10.1111/ijac.13782
39. Pazhouheshgar A, Haghighatfar Y, Moghanian A (2020) Finite element method and analytical analysis of static and dynamic pull-in instability of a functionally graded microplate. J Vib Control 28:425–438. https://doi.org/10.1177/1077546320980208
40. Saatchi A, Arani AR, Moghanian A, Mozafari M (2020) Synthesis and characterization of electrospun cerium-doped bioactive glass/chitosan/polyethylene oxide composite scaffolds for tissue engineering applications. Ceram Int. https://doi.org/10.1016/j.ceramint.2020.08.130
41. Saatchi A, Arani AR, Moghanian A, Mozafari M (2021) Cerium-doped bioactive glass-loaded chitosan/polyethylene oxide nanofiber with elevated antibacterial properties as a potential wound dressing. Ceram Int 47(7):9447–9461. https://doi.org/10.1016/j.ceramint.2020.12.078
42. Shaaban KS, Alotaibi BM, Alharbi N, Alrowaili ZA, Al-Buriahi MS, Makhlouf SA, Abd El-Rehim AF (2022) Physical, optical, and radiation characteristics of bioactive glasses for dental prosthetics and orthopaedic implants applications. Radiat Phys Chem 109995:109995. https://doi.org/10.1016/j.radphyschem.2022.109995
43. Abdel Wahab EA, Shaaban KS, Yousef ES (2020) Enhancement of optical and mechanical properties of sodium silicate glasses using zirconia. Opt Quant Electron 52. https://doi.org/10.1007/s11082-020-02575-3
44. Shaaban KS, Saddeek YB (2017) Effect of MoO_3 content on structural, thermal, mechanical and optical properties of (B_2O_3-SiO_2-Bi_2O_3-Na_2O-Fe_2O_3) glass system. Silicon 9:785–793. https://doi.org/10.1007/s12633-017-9558-5
45. El-Maaref AA, Wahab EAA, Shaaban KS, El-Agmy RM (2021) Enhancement of spectroscopic parameters of Er^{3+}-doped cadmium lithium gadolinium silicate glasses as an active medium for lasers and optical amplifiers in the NIR-region. Solid State Sci 113:106539. https://doi.org/10.1016/j.solidstatesciences.2021.106539
46. El-Rehim AFA, Shaaban KS (2021) Influence of La_2O_3 content on the structural, mechanical, and radiation-shielding properties of sodium fluoro lead barium borate glasses. J Mater Sci Mater Electron 32:4651–4671. https://doi.org/10.1007/s10854-020-05204-7
47. Sayed MA, Ali AM, Abd El-Rehim AF et al (2021) Dispersion parameters, polarizability, and basicity of Lithium phosphate glasses. J Elec Materi 50:3116–3128. https://doi.org/10.1007/s11664-021-08921-9
48. Fayad AM, Shaaban KS, Abd-Allah WM, Ouis M (2020) Structural and optical study of CoO doping in Borophosphate host glass and effect of gamma irradiation. J Inorg Organomet Polym Mater 30:5042–5052. https://doi.org/10.1007/s10904-020-01641-3
49. El-Maaref AA, Badr S, Shaaban KS, Abdel Wahab EA, Elokr MM (2019) Optical properties and radiative rates of Nd^{3+} doped zinc-sodium phosphate glasses. J Rare Earths 37:253–259. https://doi.org/10.1016/j.jre.2018.06.006
50. Abdel Wahab EA, El-Maaref AA, Shaaban KS, Börcsök J, Abdelawwad M (2021) Lithium cadmium phosphate glasses doped Sm^{3+} as a host material for near-IR laser applications. Opt Mater 111:110638. https://doi.org/10.1016/j.optmat.2020.110638
51. Shaaban KS, Abdel Wahab EA, El-Maaref AA, Abdelawwad M, Shaaban ER, Yousef ES, Wilke H, Hillmer H, Börcsök J (2020) Judd–Ofelt analysis and physical properties of erbium modified cadmium lithium gadolinium silicate glasses. J Mater Sci Mater Electron 31:4986–4996. https://doi.org/10.1007/s10854-020-03065-8
52. El-Maaref AA, El-Agmy RM, Shaaban KS, Abdel Wahab EA (2021) Optical and spectroscopic study of Nd_2O_3-doped SBN glass in the near-infrared, visible and UV regions under pumping up-conversion emissions. Eur Phys J Plus 136. https://doi.org/10.1140/epjp/s13360-021-01798-x
53. Alrowaili ZA, Al-Baradi AM, Sayed MA, Mossad Ali A, Abdel Wahab EA, Al-Buriahi MS, Shaaban KS (2021) The impact of Fe_2O_3 on the dispersion parameters and gamma / fast neutron shielding characteristics of lithium borosilicate glasses. Optik 168259:168259. https://doi.org/10.1016/j.ijleo.2021.168259
54. Wahab EAA, Aboraia AM, Shafey AME, Shaaban KS, Soldatov AV (2021) The effect of ZrO_2 on the linear and non-linear optical properties of sodium silicate glass. Opt Quant Electron 53. https://doi.org/10.1007/s11082-021-03164-8
55. Abdel Wahab EA, Shaaban KS, Alomairy S, Al-Buriahi MS (2021) Electronegativity and optical basicity of glasses containing Na/Pb/B and their high performance for radiation applications: role of ZrO_2 nanoparticles. Eur Phys J Plus 136. https://doi.org/10.1140/epjp/s13360-021-01572-z

56. Abdel Wahab EA, Shaaban KS (2021) Structural and optical features of aluminum lead borate glass doped with Fe_2O_3. Appl Phys A 127.. https://doi.org/10.1007/s00339-021-05062-y
57. El-Rehim AFA, Ali AM, Zahran HY, Yahia IS, Shaaban KS (2021) Spectroscopic, structural, thermal, and mechanical properties of B_2O_3-CeO_2-PbO_2 glasses. J Inorg Organomet Polym Mater 31: 1774–1786. https://doi.org/10.1007/s10904-020-01799-w
58. Shaaban KS, Saddeek YB, Sayed MA, Yahia IS (2018) Mechanical and thermal properties of Lead borate glasses containing CaO and NaF. Silicon 10:1973–1978. https://doi.org/10.1007/s12633-017-9709-8
59. Wahab EAA, Al-Baradi AM, Sayed MA, Ali AM, Makhlouf SA, Shaaban KS (2022) Crystallization and radiation proficiency of transparent sodium silicate glass doped zirconia. Silicon. https://doi.org/10.1007/s12633-021-01652-w
60. Shaaban KS, Al-Baradi AM, Ali AM (2022) Physical, mechanical, and thermal characteristics of B_2O_3 - SiO_2- Li_2O -Fe_2O_3 glasses. Silicon. https://doi.org/10.1007/s12633-022-01703-w
61. Alrowaili ZA, Ali AM, Al-Baradi AM, Al-Buriahi MS, Wahab EAA, Shaaban KS (2022) A significant role of MoO_3 on the optical, thermal, and radiation shielding characteristics of B_2O_3–P_2O_5–Li_2O glasses. Opt Quant Electron 54(2). https://doi.org/10.1007/s11082-021-03447-0
62. Koubisy MSI, Shaaban KS, Wahab EAA, Sayyed MI, Mahmoud KA (2021) Synthesis, structure, mechanical and radiation shielding features of $50SiO_2$–$(48 + X)$ $Na_2B_4O_7$–$(2 - X)$ MnO_2 glasses. Eur Phys J Plus 136. https://doi.org/10.1140/epjp/s13360-021-01125-4
63. El-Rehim AFA, Shaaban KS, Zahran HY, Yahia IS, Ali AM, Halaka MMA, Makhlouf SA, Wahab EAA, Shaaban ER (2021) Structural and mechanical properties of Lithium bismuth borate glasses containing molybdenum (LBBM) together with their glass–ceramics. J Inorg Organomet Polym Mater 31:1057–1065. https://doi.org/10.1007/s10904-020-01708-1
64. Shaaban KS, Zahran HY, Yahia IS, Elsaeedy HI, Shaaban ER, Makhlouf SA, Wahab EAA, Yousef ES (2020) Mechanical and radiation-shielding properties of B_2O_3–P_2O_5–Li_2O–MoO_3 glasses. Applied physics a 126. https://doi.org/10.1007/s00339-020-03982-9
65. Alothman MA, Alrowaili ZA, Alzahrani JS, Wahab EAA, Olarinoye IO, Sriwunkum C, Shaaban KS, Al-Buriahi MS (2021) Significant influence of MoO_3 content on synthesis, mechanical, and radiation shielding properties of B_2O_3-Pb_3O_4-Al_2O_3 glasses. J Alloys Compd 882:160625. https://doi.org/10.1016/j.jallcom.2021.160625
66. Shaaban KHS, Saddeek YB, Aly K (2018) Physical properties of pseudo quaternary $Na_2B_4O_7$ – SiO_2 – MoO_3 – Dy_2O_3 glasses. Ceram Int 44:3862–3867. https://doi.org/10.1016/j.ceramint.2017.11.175
67. El-Taher A, Ali AM, Saddeek YB, Elsaman R, Algarni H, Shaaban K, Amer TZ (2019) Gamma ray shielding and structural properties of iron alkali alumino-phosphate glasses modified by PbO. Radiat Phys Chem 165:108403. https://doi.org/10.1016/j.radphyschem.2019.108403
68. Abdel Wahab EA, Shaaban KS (2021) Structural and optical features of aluminum lead borate glass doped with Fe_2O_3. Appl Phys A 127(12). https://doi.org/10.1007/s00339-021-05062-y
69. Albarzan B, Almuqrin AH, Koubisy MS, Abdel Wahab EA, Mahmoud KA, Shaaban KS, Sayyed MI (2021) Effect of Fe_2O_3 doping on structural, FTIR and radiation shielding characteristics of aluminium-lead-borate glasses. Prog Nucl Energy 141:103931. https://doi.org/10.1016/j.pnucene.2021.103931
70. Alomairy S, Alrowaili ZA, Kebaili I, Wahab EAA, Mutuwong C, Al-Buriahi MS, Shaaban KS (2021) Synthesis of Pb_3O_4-SiO_2-ZnO-WO_3 glasses and their fundamental properties for gamma shielding applications. Silicon. https://doi.org/10.1007/s12633-021-01347-2
71. Alomairy S, Al-Buriahi MS, Abdel Wahab EA, Sriwunkum C, Shaaban K (2021) Synthesis, FTIR, and neutron/charged particle transmission properties of Pb_3O_4–SiO_2–ZnO–WO_3 glass system. Ceram Int 47:17322–17330. https://doi.org/10.1016/j.ceramint.2021.03.045
72. Scannell G, Koike A, Huang L (2016) Structure and thermo-mechanical response of TiO_2-SiO_2 glasses to temperature. J Non-Cryst Solids 447:238–247. https://doi.org/10.1016/j.jnoncrysol.2016.06.018

Publisher's Note Springer Nature remains neutral with regard to jurisdictional claims in published maps and institutional affiliations.